Published in final edited form as:
J Neurochem. 2012 February ; 120(4): 586–597. doi:10.1111/j.1471-4159.2011.07595.x.

Astroglial NF-κB mediates oxidative stress by regulation of NADPH oxidase in a model of retinal ischemia reperfusion injury

David J. Barakat[1], **Galina Dvoriantchikova**[2], **Dmitry Ivanov**[2,3], and **Valery I. Shestopalov**[1,2,3]

[1]Department of Molecular, Cell and Developmental Biology, University of Miami Miller School of Medicine, Miami, FL, 33136

[2]Bascom Palmer Eye Institute, University of Miami Miller School of Medicine, Miami, FL, 33136

[3]Vavilov Institute of General Genetics RAS, Moscow, Russian Federation

Abstract

Astrocytes undergo rapid activation after injury, which is mediated in part by the transcription factor NF-κB. Consequently, activated astrocytes have been shown to induce the NF-κB regulated phagocyte NADPH oxidase (PHOX), resulting in elevated production of reactive oxygen species (ROS). We investigated the regulatory mechanisms of PHOX-induced oxidative stress in astrocytes and its non cell-autonomous effects on retinal ganglion cell (RGC) loss following retinal ischemia-reperfusion (IR) injury. To study PHOX activity and neurotoxicity mediated by *glial* NF-κB, we employed GFAP-IκBα-dn transgenic mice (TG), where the NF-κB canonical pathway is suppressed specifically in astrocytes. Our analysis showed that NF-κB activation in astrocytes correlated with an increased expression of PHOX and ROS production in primary cells and whole retinas subjected to oxygen-glucose deprivation (OGD) or IR injury. Selective blockade of NF-κB in astrocytes or application of NADPH oxidase inhibitors suppressed RGC loss in co-cultures with astroglia challenged by OGD. Furthermore, genetic suppression of astroglial NF-κB reduced oxidative stress in ganglion layer neurons *in vivo* in retinal IR. Collectively, our results suggest that astroglial NF-κB-regulated PHOX activity is a crucial toxicity pathway in the pathogenesis of retinal IR injury.

Keywords

astrocyte; NF-κB; ischemia; oxidative stress; NADPH oxidase

Introduction

Astrocytes function as regulators of critical physiological functions, including glutamate uptake and release, synapse formation, ion homeostasis and information processing in the central nervous system (CNS) (Janzer and Raff 1987; Pfrieger and Barres 1997; Schousboe and Divac 1979; Schummers *et al* 2008). As a consequence of injuries, such as ischemia reperfusion (IR), astrocytes become activated, proliferate, produce pro-inflammatory cytokines and chemokines and reactive oxygen species (ROS) (Reinehr *et al* 2007; Tezel and Wax 2000; Uno *et al* 1997). Astrocyte activation initiates both protective and neurotoxic pathways, and is increasingly associated with worsened outcomes in the injured CNS

Corresponding Author: dbarakat@med.miami.edu. To whom author correspondence should be addressed: Dr. Valery I. Shestopalov, Department of Ophthalmology, University of Miami Miller School of Medicine, 1638 NW 10th Ave, Miami, FL, 33136, Tel: 305-547-3680; Fax: 305 547-3718. vshestopalov@med.miami.edu.

The authors affirm that they have no competing interests to declare

(Abramov and Duchen 2005; Faulkner *et al* 2004; Fernandez *et al* 2007; Toft-Hansen *et al*). Recently, the transcription factor Nuclear Factor-kappaB (NF-κB) was shown to be essential for the post-injury response in astrocytes and suggested as a therapeutic target following injury (Brambilla *et al* 2005; Brambilla *et al* 2009; Quinones *et al* 2008).

NF-κB is a family of ubiquitously expressed transcription factors that control the expression of hundreds of genes involved in inflammation, immune cell activation and cell survival (Papa *et al* 2004). Recently, it was shown that mice with impaired signaling of the canonical NF-κB pathway in cells expressing GFAP have improved functional recovery after both experimental autoimmune encephalomyelitis and spinal cord injury (Brambilla *et al* 2005; Brambilla *et al* 2009). This is a well-characterized transgenic (TG) mouse model with selective suppression of aNF-κB through the expression of a truncated, degradation-deficient form of IκBα under the GFAP promoter (Brambilla *et al* 2005). Significantly, the suppression of NF-kB activation in these animals is increased proportionally to the activation of the stress-responsive GFAP promoter. This mouse line has previously been shown to inhibit activation of the NF-κB heterodimer p50/p65 specifically in astrocytes, leaving neuronal NF-κB unaffected (Brambilla *et al* 2005). The expression of the transgene is limited to astrocytes and non-myelinating Schwann cells and was not found to be expressed in tissues outside of the nervous system. Neither behavioral tests (i.e. open field and grid walk tests; proprioceptive and visually elicited reflexive placing of hind or forelimbs, forelimb grip strength assessment, balance beam test), nor retinal histology (RGC density assessment) revealed any phenotypic abnormalities caused by genetic manipulation in TG mice (Brambilla *et al* 2005; Dvoriantchikova *et al* 2009). Using this mouse model, our own group has demonstrated that inhibition of astroglial NF-κB (aNF-κB) in retinal IR injury provided significant protection of neurons in the ganglion cell layer (GCL) (Dvoriantchikova *et al* 2009). However, the mechanism by which aNF-κB mediates toxicity after CNS insults has not been determined.

Oxidative stress is a major facet of ischemic injury and is implicated in neuronal death following experimental IR injury (Chen *et al* 2009; Raz *et al* ; Yoshioka *et al*). Previously, we found that suppression of aNF-κB correlated with decreased oxidative stress and the expression of the superoxide producing enzyme: phagocyte NADPH oxidase (PHOX) subunits (Dvoriantchikova *et al* 2009). We explored the hypothesis that the activation of aNF-κB after retinal IR induces oxidative stress and facilitates neuronal injury by regulating PHOX activity. PHOX is an enzyme composed of the cytosolic regulatory subunits $p47^{PHOX}$, $p67^{PHOX}$ and $p40^{PHOX}$ and the plasma membrane subunits $gp91^{PHOX}$ and $p22^{PHOX}$, which heterodimerise to form the catalytic complex cytochrome b558. Upon stimulation, the cytosolic subunits associate with cytochrome b558 along with the small GTPase, Rac1. Once assembled, the functional enzyme utilizes electrons from NADPH to reduce molecular oxygen to the free radical superoxide. It has been reported that excessive activity of PHOX can lead to oxidative damage and cell death (Li *et al* ; Park *et al* 2007). PHOX is expressed by astrocytes and neurons, and has been implicated in the pathogenesis of IR injury (Abramov *et al* 2005; Chen *et al* 2009).

The purpose of this study was to evaluate the mechanisms by which aNF-κB facilitates enhanced ROS production, oxidative stress and cell death in retinal IR injury. Analysis of cell death *in vitro* showed a direct toxic effect of aNF-κB on both astrocytes and co-cultured neurons. Retinal IR injury caused enhanced ROS synthesis, DNA and RNA damage in retinal neurons, which was blocked by genetic suppression of aNF-κB. Overall, our results reveal a pivotal role for aNF-κB in retinal IR injury and support a model where aNF-κB-regulated activity of PHOX represents a major source of ROS and cytotoxicity in the post-ischemic retina.

Experimental Procedures

Animals

All experimental procedures were performed in compliance with the NIH Guide for the Care and Use of Laboratory Animals and according to the IACUC approved protocols. GFAP-IκBα-dn transgenic mice were generated on a C57BL/6 X SJL background and backcrossed to wild type C57BL/6 mice for at least 16 generations to establish transgenic lines (Brambilla *et al* 2005). All animals used in our experiments were 3-month-old male mice or early postnatal pups (7–10 days), obtained by breeding heterozygous GFAP-IκBα-dn males with WT females. C57BL/6J-*Ncf1*^{m1J}/J animals, which lack functional expression of p47^{PHOX} protein were obtained from The Jackson Laboratory. WT littermates were used as controls.

Cell cultures

To obtain primary retinal ganglion cells (RGCs), early postnatal mouse pups were euthanized, eyes were enucleated, and retinas were mechanically dissected out. RGCs were isolated by the two-step immunopanning method (20). Briefly, whole retinas were digested in papain (8.25 U/ml, Worthington Biochemicals, Lakewood, NJ). Then, macrophages and endothelial cells were removed from the cell suspension by panning with anti-macrophage antiserum (Accurate Chemical, Westbury, NY). The RGCs bound specifically to the panning plates containing anti-Thy1.2 antibody and were released by incubation with trypsin. RGCs were grown in Neurobasal/B27 media (Invitrogen, Carlsbad, CA) containing L-gluatmine (2mM), sodium pyruvate (1mM), insulin (50ng/ml), SATO supplement, tri-iodothyronine (1ng/ml), forskolin (10ng/ml), brain derived neurotrophic factor (50ng/ml) and ciliary neurotrophic factor (10ng/ml). For RGC-astrocyte co-cultures, a monolayer of 20,000 astrocytes was plated into 96 well plastic tissue culture plates; 24 hours later, 10,000 retinal ganglion cells were plated on top of the confluent astrocytes. Experiments were performed two days after plating RGCs.

Cortical astrocytes were obtained by the “shaking method” as previously described (McCarthy and de Vellis 1980). Briefly, mouse cortices from early postnatal pups (2–5 days) were dissected and digested for one hour in papain (20U/ml). The digested tissue was triturated and plated onto plastic dishes in Dulbecco’s Modified Eagle Medium containing 10% fetal bovine serum and L-glutamine. After growing cells to confluence (approximately ten days) they were shaken overnight, washed thoroughly and tested for microglia contamination by immunostaining for the microglial marker CD11b. Cell cultures were approximately 90–95% GFAP positive cells; CD11b-positive cells were typically less than 2% of all cells (Suppl. Fig. S1).

Oxygen and glucose deprivation

Hank’s balanced salt solution (HBSS) containing 1.26 mM calcium chloride, 0.493 mM magnesium chloride, 0.407 mM magnesium sulfate, 5.33 mM potassium chloride, 0.441 mM potassium phosphate monobasic, 4.17 mM sodium bicarbonate, 137.93 mM sodium chloride, 0.338 mM sodium phosphate dibasic, and 10 mM HEPES was bubbled with 95% N_2/5% CO_2 for 15 minutes for deoxygenation. Growth media was removed and cells were washed twice with HBSS and then deoxygenated HBSS was added. Astroglial primary cultures were then placed in a hypoxic chamber with 95% N_2/5% CO_2 entering the chamber until the oxygen tension reached 0.5%. Cells were maintained in the hypoxic chamber for 4 hours and the media was replaced with fresh growth medium and returned to a normoxic humidified CO_2 incubator. To assess changes at the gene expression level, cells were sampled within 12 hours after the return to normoxia; a 24 hour time point was used in the experiments assessing cell death.

Preparation of conditioned media

Primary astrocytes were plated in 12 well plates and allowed to reach confluence. Growth media was removed and cells were washed twice with glucose free HBSS or HBSS containing glucose in control cultures. Astrocytes cultures were then incubated for four hours in a hypoxic chamber, controls were incubated in normoxic conditions with glucose. The conditioned media was then collected, supplemented with 10mM glucose and used immediately for neuronal treatment.

Transient retinal ischemia

Retinal ischemia was induced for 60 minutes by introducing into the anterior chamber of the eye a 33-gauge needle attached to a normal (0.9% NaCl) saline-filled reservoir raised to increase intraocular pressure (IOP) (IOP increased to 120 mm Hg). The contralateral eye was cannulated and maintained at normal IOP to serve as a normotensive control. Body temperature was maintained at 37 ± 0.5°C. Complete retinal ischemia, evidenced by a whitening of the anterior segment of the eye and blanching of the retinal arteries, was verified by microscopic examination.

Real-time PCR: Real-time PCR

Real-time PCR analysis was performed using gene-specific primers. For ActB forward: CACCCTGTGCTGCTCACC, and reverse: GCACGATTTCCCTCTCAG; $p47^{PHOX}$ forward: CGAGAAGAGTTCGGGAACAG and reverse: AGCCATCCAGGAGCTTATGA; $p67^{PHOX}$ forward: CTTCAACATAGGCTGCGTGA and reverse: CTTCATGTTGGTTGCCAATG; $p40^{PHOX}$ forward: TCAGAGAGCGACTTTGAGCA; and reverse: GTTTTGCGCCATGTAGACT; $p22^{PHOX}$ forward: AAAGAGGAAAAAGGGGTCCA and reverse: CTCCTCTTCACCCTCACTCG; $gp91^{PHOX}$ forward: GACTGCGGAGAGTTTGGAAG, and reverse: ACTGTCCCACCTCCATCTTG. Total RNA was extracted from astrocytes using Trizol (Invitrogen, Carlsbad, CA) and reverse transcribed with the Reverse Transcription System (Promega, USA) to synthesize cDNA. Real time PCR was performed with the Rotor-Gene 6000 Cycler (Corbett Research, Australia) using the SYBR GREEN PCR MasterMix (Qiagen, USA). For each gene, the relative expression was calculated by comparison with a standard curve, following normalization to the housekeeping gene β-actin (*Actb*) as control.

Immunohistochemistry

Cultured cells were fixed in 4% paraformaldehyde solution (PF) in PBS pH 7.4 and blocked with 10% normal goat serum with 0.3% triton-x 100 in PBS at pH 7.4. Cells were then incubated with FITC conjugated anti-NeuN (Milipore, 1:150), FITC conjugated beta III tubulin or anti-active caspase-3 (Cell Signaling Technology, 1:250), which recognizes the activated, cleaved 17kD form of caspase-3 but shows no specificity to the full length inactive pro-enzyme. The cells were then incubated with goat anti-rabbit alexafluor546 (Invitrogen, Carlsbad, CA; 1:500) for 1 hour for fluorescence. Negative controls were incubated with secondary antibody only.

For IHC in flatmounted retinas, eyes were enucleated after euthanasia, incised at the ora serrata, and immersion-fixed in a 4% PF solution in PBS (pH 7.4) for 1 hour. The retinas were then removed and cryoprotected overnight in 30% sucrose. The retinas were then freeze-thawed 3 times and rinsed 3×10 minutes in 0.1 M PB buffer at pH 7.4. DNA in the retinas was denatured with 2N HCl for 30 minutes, and the retinas were blocked by exposure to 5% donkey serum, 0.1% Triton X-100 in 0.1M tris buffer (TB) for 1 hour. The retinas were then incubated overnight with anti-8-hydroxyguanosine (1:1000, QED Bioscience Inc, San Diego, CA), anti-GFAP (Sigma, 1:400), anti-$p47^{PHOX}$ (1:200), or

monoclonal FITC-conjugated NeuN antibody (Chemicon/Invitrogen, USA; dilution 1:150). To label the cells, goat anti-mouse AlexaFluor 546 IgG2a (Invitrogen, Carlsbad, CA; 1:500) or donkey anti-rabbit 647 (Invitrogen, Carlsbad, CA; 1:500) was applied for 2 hours, and the nuclei were made visible by addition of Hoechst 3342 (1ug/ml). After washing with 0.1M TB, retinas were flatmounted and coverslipped. Negative controls were incubated in secondary antibody only.

Counting NeuN/8-hydroxyguanosine-positive GCL neurons

The DNA/RNA damage was detected microscopically as co-localization of Hoechst/NeuN/8-OH-guanosine labeling. The stained sections were examined with a Leica TSL AOBS SP5 confocal microscope at 400× magnification under oil immersion (Leica Microsystems, PA). Individual retinas were sampled randomly to collect 12 quality images of standard microscopy fields. Images were captured in four retinal quadrants at the same eccentricity from the optic disc in the central, middle and peripheral retina. The total numbers of NeuN/Hoechst/8-hydroxyguanosine positive cells with a typical to RGCs size range of 6 to 30 μm were counted in 4 fields corresponding to each of the three regions after image thresholding and manual exclusion of artifacts using MetaMorph analytical software (Molecular Devices, Sunnyvale, CA). A minimum of five animals were analyzed for each genotype or treatment condition.

Cell death assays

After oxygen-glucose deprivation (OGD), the number of necrotic and apoptotic cells were determined with the Vybrant Apoptosis Assay Kit #2 (Invitrogen, Carlsbad, CA). The percentages of necrotic cells (Propidium Iodide (PI) positive or both Annexin V and PI positive) and apoptotic cells (only AnnexinV-positive) relative to the total number of cells examined were determined for each of the five non-overlapping randomly selected fields. For co-culture experiments, cell death was detected by the co-expression of active caspase-3 (Cell Signaling Technology; 1:200) and FITC-conjugated NeuN (Milipore; 1:150) or FITC conjugated beta III tubulin (Abcam, 1:200) by IHC. The percentage of active caspase-3 and NeuN positive cells relative to the total number of NeuN positive cells was determined.

Gene knockdown

$p47^{PHOX}$ siRNA or control non-targeting siRNA (Santa Cruz Biotechnology, Santa Cruz, CA) was incubated with of Lipoectamine RNAiMAX (Invitrogen, Carlsbad, CA) transfection reagent in individual wells of cell culture plates at a ratio of 10pmol siRNA duplex: 1.5μL lipofectamine RNAiMAX with a final concentration of 100nM siRNA after addition of cells and media. siRNA targeting p47 was premade and consisted of a pool of three target specific siRNAs designed for knockdown of gene expression (Santa Cruz Biotechnology). Non-targeting control siRNA consists of a 20–25 nucleotide RNA oligomer with a scrambled sequence that was designed by the manufacturer and will not target any known cellular mRNAs (Santa Cruz Biotechnology). Primary astrocytes in DMEM containing 10% FBS were plated into individual wells containing transfection reagent and siRNA duplex and incubated for 24 hours at 37° in a 5% CO_2 incubator then washed and replaced with growth media. Cell toxicity of siRNA treatment was determined by PI staining 48 hours post transfection. The rate of cell death in siRNA-treated cells relative to media-only controls was insignificantly different (Suppl. Fig. S2). Less than 1% of cells in control or siRNA treated cultures were positive for PI labeling.

Western blot analysis

20 μg of protein extract containing protease and phosphatase inhibitors cocktail were loaded into precast 4–12% Bis-Tris gels (Invitrogen, Carlsbad, CA) and the proteins were size-

separated by SDS-polyacrylamide gel electrophoresis. Proteins were transferred onto PVDF membranes (Invitrogen, Carlsbad, CA) and incubated with anti-gp91^{PHOX} (BD Transduction Laboratories, 1:1000), anti-p47^{PHOX} (Santa Cruz Biotechnology, 1:500), or anti-β-actin (Sigma, 1:2500), anti-phospho p47^{PHOX} (Assay Biotechnology; 1:1000). Proteins recognized by the antibodies were made visible by the SuperSignal West Femto Maximum Sensitivity Substrate from Pierce according to manufacturer instructions (Thermo Fisher Scientific, Rockford, IL). Chemiluminescent signals were detected by ImageQuant LAS 4000 Biomolecular Imager (GE Healthcare) equipped with a cooled CCD camera. Quantification of the protein band density was carried out using the software program ImageJ. *Detection of reactive oxygen species (ROS):* Superoxide was detected *in vitro* with the Diogenes Cellular Luminescence Enhancement System according to the manufacturer's instructions. Briefly, the Diogenes reagent was added to live astrocytes cultured in DPBS with calcium, sodium pyruvate, and glucose, and the intensity of luminescence was quantified with a Lumistar Optima luminometer. For baseline recordings, chemiluminescence was measured every 5 seconds for 2 minutes/sample. To measure the enzymatic activity of PHOX, we applied phorbol myristate acetate (PMA) to astrocytes in culture. Astrocytes were treated with PMA (1ug/ml, Sigma) for twenty minutes, and the intensity of the chemiluminescence was quantified every 5 seconds for 2 minutes/sample. The average chemiluminescent output was recorded every six minutes. Superoxide dismutase (10U/ml) was added to the cells to quench extracellular superoxide production. ROS were detected *in vivo* by dihydroethidium (DHE). Unfixed retinas were mounted in OCT medium and frozen on dry ice. Then 20 μm frozen cryostat sections were cut, washed with PBS, and incubated at 37°C for 15 minutes in DHE (5ug/ml) with or without apocynin (100μM). Sections were immediately examined by confocal microscopy using a 488 excitation wavelength to detect 2-OH-ethidium-specific fluorescence.

Statistical analysis

Statistical analysis was performed by one-way ANOVA followed by Tukey test for multiple comparisons. In single comparisons, the Student's *t* test was used. *P* values equal to or less than 0.05 were considered statistically significant.

Results

aNF-κB induces oxidative stress in the ganglion cell layer after IR injury

Previously we have shown that suppression of aNF-κB promotes the survival of ganglion cell layer neurons after IR injury and this protection was correlated with a decrease in oxidative stress of the entire retina (Dvoriantchikova *et al* 2009). To evaluate whether aNF-κB can facilitate oxidative stress in the retina *in vivo*, we compared ROS accumulation 24 hours after retinal IR by probing unfixed retinal sections with dihydroethidium (DHE). Upon oxidation to 2-hydroxy-ethidium (2-OH-Et), this dye binds to DNA and exhibits excitation and emission wavelengths distinct from DHE, which are captured by confocal microscopy. Our analysis showed that WT but not TG retinas displayed enhanced fluorescence intensity of the oxidized 2-OH-Et indicator dye 24 hours after reperfusion (Suppl. Fig. S3). To control the specificity of the fluorescent signal, we applied the NADPH oxidase inhibitor apocynin directly to frozen retinal sections prior to measurements, which resulted in abrogated 2-OH-Et fluorescence. Next, we determined whether enhanced ROS production correlated with aNF-κB activity and oxidative stress in the ganglion cell layer (GCL). We assayed neurons in the GCL for oxidative stress by probing for DNA and RNA damage 72 hours after IR injury using anti-8-OH-guanosine antibodies. The analysis using direct counting of double-labeled NeuN/8-OH-guanosine positive cells at the center, middle and periphery of the retina revealed significantly greater numbers of damaged neurons in WT relative to TG retinas (Figs. 1A and B). These data indicate that genetic suppression of aNF-κB has

decreased DNA/RNA damage in retinas exposed to IR injury. Combined, these results imply that the activity of aNF-κB is involved in the regulation of ROS production by NADPH oxidase and contributes to post-IR oxidative damage to retinal neurons*in vivo*.

aNF-κB facilitates RGC death by activation of neuronal PHOX

Our analysis of the neurotoxic effects of aNF-κB on retinal neurons allowed us to hypothesize that astrocytes could facilitate endogenous PHOX-mediated oxidative stress in RGCs. We tested whether OGD-challenged astrocytes affect RGC survival and increase neuronal ROS production in controlled *in vitro* conditions. First, we assayed RGC survival in astrocyte-neuron co-cultures in which purified RGCs were plated directly on an astrocyte monolayer. The number of activated caspase-3/NeuN positive RGCs were counted 24 hours after OGD challenge. We utilized an antibody that specifically recognizes the cleaved, active form of caspase-3, but has no affinity to the inactive pro-enzyme. We observed an approximately 2-fold increase in the rate of cell death in RGCs co-cultured with WT vs. TG astrocytes (Fig. 2A and Suppl. Fig. S4A). Next, to test whether neuronal PHOX activity plays a role in the astrocytes-induced RGC loss, we quantified cell death rates in OGD-challenged RGC-astrocyte co-cultures with and without pharmacological blockade of NADPH oxidase. The application of the NADPH oxidase inhibitors diphenylene iodonium chloride (DPI) or apocynin significantly reduced RGC death in these co-cultures (Figure 2B and Suppl. Fig. S4B). Similarly, we found that in co-cultures with RGCs lacking functional PHOX due to a spontaneous mutation of $p47^{PHOX}$ ($p47^{null}$) subunit, these neurons were significantly protected from OGD-induced apoptosis (Fig. 2C). Finally, we tested whether OGD-treated astrocytes can facilitate PHOX-dependent RGC death without direct contact, i.e. through the release of soluble factors into the environment. Astrocyte-conditioned media (ACM) from cells exposed to OGD for four hours (OGD ACM) was used to treat primary RGC cultures, control RGCs were treated with ACM collected from normoxia treated astrocytes (control ACM). We counted the number of PI/Hoechst positive and Annexin V/Hoechst positive RGCs to determine dead and apoptotic cells respectively. The treatment with OGD ACM but not control ACM caused an increase in the rate of WT RGC death observed at six hours of exposure (Fig. 2D and Suppl. Fig. S5). $p47^{null}$ RGCs showed no increase above the baseline rate of cell death with the same treatment. These findings confirmed our hypothesis that OGD-challenged astrocytes release soluble factors that facilitate RGC loss through the induction of neuronal PHOX.

$p47^{PHOX}$is transcriptionally activated after OGD

Our previous (Dvoriantchikova *et al* 2009) and current findings demonstrate a relationship between NF-κB, NADPH oxidase and oxidative stress in retinal IR injury. Furthermore, earlier studies have shown PHOX subunits to be regulated by NF-κB mediated transcription in other cell types (Anrather *et al* 2006; Gauss *et al* 2007). To test the hypothesis that NF-κB regulates the transcription of PHOX genes in ischemia, we first examined whether the PHOX genes $p47^{PHOX}$ and $gp91^{PHOX}$ were induced after OGD in primary cortical astrocytes. We challenged astrocytes for 4 hours by OGD, and collected RNA 6, 9 and 12 hours after the return to normoxic growth medium with glucose. Quantitative RT-PCR (qPCR) analysis of RNA from astrocytes subjected to OGD showed a time-dependent increase in expression of the $p47^{PHOX}$ and $gp91^{PHOX}$ genes, which significantly increased at 12 hours post-OGD (Figs. 3A, B). We further utilized this time point to distinguish whether the increase in $p47^{PHOX}$ transcript abundance was due to higher stability or elevated transcriptional activity. We treated cells with the transcriptional inhibitor actinomycin D (5μg/ml) at 12 hours after OGD, and extracted RNA thirty, sixty and one hundred twenty minutes after the treatment. The expression of $p47^{PHOX}$ was decreased to approximately fifty percent 30 minutes after the actinomycin D treatment and remained at this level for the duration of the experiment (Fig. 3C). The addition of the protein synthesis inhibitor

cycloheximide (5μg/ml), which is also known to block degradation of some mRNAs, stabilized $p47^{PHOX}$ transcripts (Fig. 3C). To further assess the regulation of $p47^{PHOX}$ we analyzed the transcript levels 12 hours after OGD challenge in the presence or absence of cycloheximide. Indeed, we observed a dramatic 5-fold increase in $p47^{PHOX}$ transcripts in post-OGD astrocyte cultures pre-treated with cycloheximide (Fig. 3D). Control cultures, treated with cycloheximide in normoxia, showed $p47^{PHOX}$ transcript levels similar to that observed in the vehicle-treated cells. Taken together, these data indicate that PHOX is transcriptionally regulated in astrocytes challenged by OGD.

NF-κB regulates homeostatic levels of PHOX in primary astrocytes

We next asked whether aNF-κB regulates PHOX transcription after OGD. First, we tested whether up-regulation of $p47^{PHOX}$ and $gp91^{PHOX}$ was NF-κB dependent. We challenged WT and TG astrocytes by OGD and analyzed gene expression by qPCR 12 hours after return to normoxia. Similar to the results of prior experiments, WT astrocytes showed a marked increase in transcript levels of both $p47^{PHOX}$ and $gp91^{PHOX}$, but upregulation of both $gp91^{PHOX}$ and $p47^{PHOX}$ was blocked in TG astrocytes (Fig. 4A). To determine whether these increases in transcripts correlated with levels of PHOX proteins, we analyzed cell extracts from astrocyte cultures for $p47^{PHOX}$ and $gp91^{PHOX}$ by quantitative Western blotting (Fig. 4B). Contrary to our expectations, there was no change in total $p47^{PHOX}$ or $gp91^{PHOX}$ protein levels within 24 hours after OGD in either WT or TG astrocytes. However, we detected significant differences in the levels of $gp91^{PHOX}$ and $p47^{PHOX}$ proteins in TG vs. WT astrocytes (Figs. 4B, C; $n=3$, $p<0.01$). Furthermore, using immunohistochemistry in fixed retinal slices, we found that increased $p47^{PHOX}$-specific immunostaining co-localized with GFAP positive astrocytes in WT but not in TG retinas (Suppl. Fig. S6).

These findings prompted us to compare untreated wild type (WT) and TG astrocytes for basal levels of PHOX subunit gene expression. We found that TG astrocytes express significantly lower basal levels of $p22^{PHOX}$ and $p40^{PHOX}$ and similar levels of $gp91^{PHOX}$, $p47^{PHOX}$ and $p67^{PHOX}$ transcripts relative to WT (Fig. 4D). These data suggest that NF-κB activity constitutively regulates PHOX protein levels in astrocytes.

ROS production by PHOX is regulated by aNF-κB

To test whether differences in PHOX protein levels between WT and TG astrocytes corresponded to increased PHOX activity, as measured by superoxide production, we assayed astrocytes by Diogenes luminescence 24 hours after OGD challenge. WT astrocytes exhibited a significantly greater induction in superoxide production by OGD relative to TG astrocytes (Fig. 5A).

Using a siRNA-mediated knockdown approach, we tested whether PHOX, and not other enzymes, was the source of increased ROS after OGD. We transfected astrocytes with either scrambled control RNA or siRNA specifically targeting $p47^{PHOX}$. The siRNA –induced knock down of $p47^{PHOX}$ was confirmed at the protein level by western blot 48 hours post transfection with 100nm $p47^{PHOX}$ siRNA (Fig. 5B). The level of ROS production decreased significantly after OGD in $p47^{PHOX}$ siRNA treated cells, but not in cells transfected with control RNA (Fig. 5C). These data imply that the majority of extracellular ROS in astrocytes is produced by PHOX.

Both resting and OGD treated astrocytes displayed low levels of extracellular ROS production. To further evaluate enzymatic activity of PHOX in astrocytes we therefore applied a potent PHOX activator, the diacylglycerol analogue PMA (Abramov *et al* 2005). We added PMA to both untreated and OGD challenged astrocytes and assayed ROS

production after 20 minutes of exposure using Diogenes reagent. To show specificity for superoxide, superoxide dismutase (SOD) was added to cultures to quench chemiluminescence. Both TG and WT cells showed a two fold increase in ROS production after OGD treatment. However, as compared to TG cells, WT cells exhibited approximately ten-fold greater output of ROS after PMA stimulation. These data imply that differences between genotypes in gross production of ROS are consistent with differences in basal levels of PHOX protein expression, rather than with the degree of induction by OGD. Furthermore, relative increases in ROS production in WT and TG cells 24 hours after OGD challenge suggest that the increase in ROS production following OGD is independent of NF-κB (Figs. 5A and D).

PHOX assembly and activation requires $p47^{PHOX}$ phosphorylation (Raad *et al* 2009). To test whether levels of $p47^{PHOX}$ protein phosphorylation change after OGD treatment, we analyzed cell lysates by Western blot with antibodies specific to phospho-$p47^{PHOX}$ protein. We did not detect a significant difference in phospho-$p47^{PHOX}$ levels between cells with or without PMA stimulation at 24 hours after OGD (Fig. 5F). Our data indicated that $p47^{PHOX}$ was already phosphorylated in untreated cells and the phosphorylation levels did not change after OGD. These results suggest that NF-κB regulates PHOX activity at homeostatic levels and this is crucial for the rate of ROS output in astrocytes. The post-ischemic increase of ROS production by this enzyme, however, is regulated independently of NF-κB.

Finally, we tested whether astrocyte survival was influenced by NF-κB suppression because astrocyte demise was shown to pose an additional challenge to the injured CNS (Zhao and Rempe 2010). We analyzed percentages of apoptotic and dead astrocytes in WT and TG cultures detected by PI and AnnexinV staining 24 hours after OGD challenge. The rate of OGD-induced cell death was significantly higher in cultures of WT (31±9%) compared to TG (6±3%) astrocytes (Figs. 6A,B). Apoptotic cells were relatively scarce in both cultures. Significantly, the cell death rate in OGD-challenged WT cultures was reduced by treatment with the NADPH oxidase inhibitor DPI (Fig. 6C). The demise of astrocytes following OGD is, therefore, facilitated by aNF-κB and, at least partially, through the activation NADPH oxidase.

Discussion

In this study we obtained experimental evidence for the crucial role of aNF-κB in the regulation of PHOX activity and cell death. In turn, the activity of PHOX proved to be a major contributor to oxidative stress, DNA/RNA damage and neuronal death in the two models of neuronal IR injury. The GFAP-IκB-dn mouse line with genetically suppressed astroglial NF-κB activation allowed us to attribute the neurotoxicity data generated in ischemic conditions specifically to the activity of astroglial NF-κB. In contrast to other strategies aiming to achieve genetic suppression of NF-κB, such as the p50 subunit deficiency associated with immunological deficits, autoimmunity and degenerative disease (Lu *et al* 2006; Takahashi *et al* 2007), GFAP-IκB-dn mice possess no detectable phenotype in physiological conditions at all ages examined. Our previous results (Brambilla *et al* 2009; Dvoriantchikova *et al* 2009) and data from other studies (Brambilla *et al* 2005; Saijo *et al* 2009) have provided strong evidence for a causative relationship between aNF-κB activity, inflammation, and neuronal injury in different CNS injury models.

It is known that NF-κB functions can vary considerably depending on the cell type, but multiple studies in the ischemic CNS have shown that NF-κB activation is neurotoxic (Duckworth *et al* 2006; Li *et al* 2008; Schneider *et al* 1999). Our data obtained in this study suggest that, at least in part, this effect is due to the NF-κB-induced increase in PHOX activity. We have previously shown that aNF-κB facilitates neuronal loss in the retinal

ganglion cell layer after IR (Dvoriantchikova *et al* 2009). The analysis of *in vitro* caspase-3 activation and AnnexinV labeling data generated here showed that astrocytes require activation of NF-κB in order to facilitate RGC death in co-cultures. This is significant because apoptosis occurs secondary to injury and thus the suppression of NF-κB likely blocked critical signals triggering RGC death in culture. Another evidence of a noxious effect of aNF-kB-dependent glia-neuron signaling event(s) is that such toxicity was observed either with or without direct glia-neuron contact. Furthermore, our data showed that conditioned media from OGD challenged astrocytes facilitated RGC death through activation of PHOX. Both pharmacological NADPH oxidase inhibitors and genetic blockade of $p47^{PHOX}$ subunit protected RGCs in co-cultures with astrocytes exposed to OGD challenge. We, therefore, suggested a model where activation of aNF-κB modulates the release of factor(s) that facilitate RGC death in a non-cell-autonomous fashion, through activation of neuronal PHOX. Our experiments demonstrating reduced oxidative stress in GCL and ROS production throughout the retina in TG vs. WT mice support this model. Thus, we found that ganglion layer neurons of the central retina were particularly susceptible to IR-induced DNA/RNA damage, which was blocked by suppressing aNF-κB. One possible explanation of such “geographic” degeneration is a greater density of astrocytes in this region of the retina and a higher cumulative impact via facilitating activation of neuronal PHOX and subsequent oxidative stress. Indeed, it has been shown that injuries incurred by ischemia or elevated intraocular pressure in the retina induce the release of several PHOX activating compounds, including glutamate analogues, necrotic factors and ATP, which accumulate in the extracellular space in ischemic or pressure induced retinal injuries (Brennan *et al* 2009; Kampfrath *et al* 2011; Liu *et al* 2006; Moore and MacKenzie 2009; Reigada *et al* 2008). Additional factor contributing to a differential impact in the central vs. peripheral retina could be a longer time needed to deplete oxygen and ATP below levels critical for the survival at the *periphery*, where neuronal density is lower.

We found that astrocyte cultures with impaired canonical NF-κB signaling were significantly protected from OGD *in vitro*, which also correlated with a reduction in PHOX activity. Similar results were reported by Lee and co-authors following OGD in astrocytes with siRNA knockdown of the p50 NF-κB subunit (Lee *et al* 2006). It stands to reason that NF-κB -regulated basal PHOX protein levels is essential to the potency of PHOX-mediated ROS production causing oxidative stress and cell death of astrocytes after OGD. However, chemical inhibition of PHOX in our experiments did not result in near-complete rescue of astrocytes as we observed in TG cell cultures. It is likely that cell death in astrocytes is mediated by several pathways downstream of NF-κB. Furthermore, these results raise the possibility that reduced astrocyte cell death rate or lower levels of PHOX activating ligands in TG animals are responsible for attenuated PHOX activation in RGCs. Further studies are required to define the nature of astrocyte-neuron signaling implicated in neuronal PHOX activation.

It has been established that PHOX is a NF-κB-regulated complex in phagocytes (Anrather et al 2006). In agreement with this model, we detected that transcription of PHOX genes after OGD is NF-κB-dependent in astrocytes. However, chronic suppression of NF-κB activity in TG astrocytes resulted in significantly decreased basal levels of two PHOX-encoding genes, $p40^{PHOX}$ and $p22^{PHOX}$, and PHOX proteins. These results provide a plausible explanation for constitutively lowered levels of PHOX proteins in TG vs. WT cells and retinas. Consistent with our findings, it was recently demonstrated that suppression of Akt/NF-κB signaling reduced levels of $p22^{PHOX}$ in pancreatic cancer cell lines (Edderkaoui *et al*). Furthermore, insufficiency of the $p22^{PHOX}$ subunit causes degradation of $gp91^{PHOX}$, since stability of $gp91^{PHOX}$ is dependent on the formation of a heterodimer with its partner $p22^{PHOX}$ (DeLeo *et al* 2000; Maly *et al* 1993; Yu *et al* 1997). It is therefore reasonable to suggest that NF-κB regulates homeostatic levels of PHOX proteins and has a critical

functional role before ischemic injury ensues. Thus, activation of PHOX, without increases in protein levels, in IR and OGD conditions should result in greater ROS production and oxidative injury in WT relative to TG animals. This is exactly what we observed in our current experiments and in previous studies in the retinal IR model (Dvoriantchikova *et al* 2009).

Counter to our expectations, we found that OGD had no effect on the levels of total PHOX proteins within 24 hours after exposure. One possibility for the lack of a corresponding increase in PHOX proteins could be a limited availability of heme, which is required for gp91 biosynthesis (Yu *et al* 1997). Following OGD, a depletion of the available heme pool that interferes with gp91 biosynthesis in astrocytes could occur due to strong upregulation of the antioxidant enzyme, heme oxygenase-1 (HO-1), which cleaves heme to generate biliverdin (Imuta *et al* 2007). Indeed, an over-expression of HO-1 was shown to result in reduced gp91 protein abundance in macrophages (Taille *et al* 2004). Thus, the competition for heme between HO-1 and PHOX could prevent the accumulation of PHOX proteins in astrocytes despite transcriptional upregulation.

Our data showed that the 2-fold increase in PHOX-mediated ROS production in astrocytes challenged by OGD was independent of both transcriptional regulation by NF-κB and PHOX protein abundance. It is known, that enzymatic activity of PHOX can be regulated by several factors, including phosphorylation status, intracellular Ca^{2+} and protein kinase C beta (PKCβ) activity. Our results discounted the role of phosphorylation, since the levels of the phospho-$p47^{PHOX}$ subunit remained unchanged after PMA treatment. These data are consistent with the results published by Abramov et al. (Abramov *et al* 2005), who reported that in astroglia PHOX is preassembled into active complexes and does not require additional phosphorylation. Therefore, enhanced PKCβ activity or calcium influx after OGD are more likely to facilitate NF-κB independent regulation of PHOX activity in astrocytes, because both are increased by PMA stimulation.

In conclusion, we found that aNF-κB is a critical regulator of PHOX-induced oxidative stress in retinal IR injury. The suppression of aNF-κB rescued primary astrocytes and neurons from OGD induced death *in vitro* and suppressed IR-induced ROS production in the entire retina *in vivo*. We found that, aNF-κB regulation of PHOX activity is twofold in that 1) aNF-κB facilitates PHOX activity by transcriptional regulation of homeostatic PHOX levels in astrocytes and 2) the activation of aNF-kB following IR injury activates neuronal PHOX through the release of soluble factors into the extracellular space. Intriguingly, chronic inhibition of aNF-κB suppressed PHOX protein expression in naive cells and retinas; suggesting that aNF-κB plays a critical role before IR injury occurs. This study provides new insights on the deleterious role that astrocytes play in ischemic retinal injury. Our results strongly suggest that NF-κB and downstream pathways in astroglia are valid targets for neuroprotective interventions in retinal ischemia.

Supplementary Material

Refer to Web version on PubMed Central for supplementary material.

Abreviations used in text

ACM	astrocyte conditioned media
PHOX	phagocyte NADPH oxidase
GCL	ganglion cell layer

TG	Transgenic
WT	wild type
OGD	oxygen glucose deprivation
RGC	retinal ganglion cell
IR	ischemia-reperfusion
ROS	reactive oxygen species
CNS	central nervous system
NF-κB	nuclear factor-kappaB
DHE	dihydroethidium
2-OH-ET	2-hydroxy-ethidium
DPI	diphenyline iodonium chloride
PMA	phorbol-myristate acetate
HO-1	heme oxygenase-1

Acknowledgments

This study was supported by NIH grant EY017991 and Research to Prevent Blindness (RPB) Career Development Award (V.S.); NEI grant R21EY020613 and AHA Scientist Development Award 0735014B (D.I.); NIH grant P30 EY014801 and an unrestricted RPB grant to the Department of Ophthalmology, University of Miami. The content is solely the responsibility of the authors and does not necessarily represent the official views of the National Eye Institute or the National Institutes of Health.

*We thank Dr. John R. Bethea for providing us with GFAP-IkB-dn transgenic mice, Dr. T. Lampidis for providing us with the hypoxic chamber and Gabriel Gaidosh for his expert assistance in microscopic analysis.

References

Abramov AY, Duchen MR. The role of an astrocytic NADPH oxidase in the neurotoxicity of amyloid beta peptides. Philos Trans R Soc Lond B Biol Sci. 2005; 360:2309–2314. [PubMed: 16321801]

Abramov AY, Jacobson J, Wientjes F, Hothersall J, Canevari L, Duchen MR. Expression and modulation of an NADPH oxidase in mammalian astrocytes. J Neurosci. 2005; 25:9176–9184. [PubMed: 16207877]

Anrather J, Racchumi G, Iadecola C. NF-kappaB regulates phagocytic NADPH oxidase by inducing the expression of gp91phox. J Biol Chem. 2006; 281:5657–5667. [PubMed: 16407283]

Brambilla R, Bracchi-Ricard V, Hu WH, Frydel B, Bramwell A, Karmally S, Green EJ, Bethea JR. Inhibition of astroglial nuclear factor kappaB reduces inflammation and improves functional recovery after spinal cord injury. J Exp Med. 2005; 202:145–156. [PubMed: 15998793]

Brambilla R, Persaud T, Hu X, Karmally S, Shestopalov VI, Dvoriantchikova G, Ivanov D, Nathanson L, Barnum SR, Bethea JR. Transgenic inhibition of astroglial NF-kappa B improves functional outcome in experimental autoimmune encephalomyelitis by suppressing chronic central nervous system inflammation. J Immunol. 2009; 182:2628–2640. [PubMed: 19234157]

Brennan AM, Suh SW, Won SJ, Narasimhan P, Kauppinen TM, Lee H, Edling Y, Chan PH, Swanson RA. NADPH oxidase is the primary source of superoxide induced by NMDA receptor activation. Nat Neurosci. 2009; 12:857–863. [PubMed: 19503084]

Chen H, Song YS, Chan PH. Inhibition of NADPH oxidase is neuroprotective after ischemia-reperfusion. J Cereb Blood Flow Metab. 2009; 29:1262–1272. [PubMed: 19417757]

DeLeo FR, Burritt JB, Yu L, Jesaitis AJ, Dinauer MC, Nauseef WM. Processing and maturation of flavocytochrome b558 include incorporation of heme as a prerequisite for heterodimer assembly. J Biol Chem. 2000; 275:13986–13993. [PubMed: 10788525]

Duckworth EA, Butler T, Collier L, Collier S, Pennypacker KR. NF-kappaB protects neurons from ischemic injury after middle cerebral artery occlusion in mice. Brain Res. 2006; 1088:167–175. [PubMed: 16630592]

Dvoriantchikova G, Barakat D, Brambilla R, Agudelo C, Hernandez E, Bethea JR, Shestopalov VI, Ivanov D. Inactivation of astroglial NF-kappa B promotes survival of retinal neurons following ischemic injury. Eur J Neurosci. 2009; 30:175–185. [PubMed: 19614983]

Edderkaoui M, Nitsche C, Zheng L, Pandol SJ, Gukovsky I, Gukovskaya AS. NADPH oxidase activation in pancreatic cancer cells is mediated through Akt dependent up-regulation of p22phox. J Biol Chem.

Faulkner JR, Herrmann JE, Woo MJ, Tansey KE, Doan NB, Sofroniew MV. Reactive astrocytes protect tissue and preserve function after spinal cord injury. J Neurosci. 2004; 24:2143–2155. [PubMed: 14999065]

Fernandez AM, Fernandez S, Carrero P, Garcia-Garcia M, Torres-Aleman I. Calcineurin in reactive astrocytes plays a key role in the interplay between proinflammatory and anti-inflammatory signals. J Neurosci. 2007; 27:8745–8756. [PubMed: 17699657]

Gauss KA, Nelson-Overton LK, Siemsen DW, Gao Y, DeLeo FR, Quinn MT. Role of NF-kappaB in transcriptional regulation of the phagocyte NADPH oxidase by tumor necrosis factor-alpha. J Leukoc Biol. 2007; 82:729–741. [PubMed: 17537988]

Imuta N, Hori O, Kitao Y, Tabata Y, Yoshimoto T, Matsuyama T, Ogawa S. Hypoxia-mediated induction of heme oxygenase type I and carbon monoxide release from astrocytes protects nearby cerebral neurons from hypoxia-mediated apoptosis. Antioxid Redox Signal. 2007; 9:543–552. [PubMed: 17330989]

Janzer RC, Raff MC. Astrocytes induce blood-brain barrier properties in endothelial cells. Nature. 1987; 325:253–257. [PubMed: 3543687]

Kampfrath T, Maiseyeu A, Ying Z, Shah Z, Deiuliis JA, Xu X, Kherada N, Brook RD, Reddy KM, Padture NP, Parthasarathy S, Chen LC, Moffatt-Bruce S, Sun Q, Morawietz H, Rajagopalan S. Chronic fine particulate matter exposure induces systemic vascular dysfunction via NADPH oxidase and TLR4 pathways. Circ Res. 2011; 108:716–726. [PubMed: 21273555]

Lee YS, Song YS, Giffard RG, Chan PH. Biphasic role of nuclear factor-kappa B on cell survival and COX-2 expression in SOD1 Tg astrocytes after oxygen glucose deprivation. J Cereb Blood Flow Metab. 2006; 26:1076–1088. [PubMed: 16395278]

Li G, Scull C, Ozcan L. Tabas I NADPH oxidase links endoplasmic reticulum stress, oxidative stress, and PKR activation to induce apoptosis. J Cell Biol. 191:1113–1125. [PubMed: 21135141]

Li J, Lu Z, Li WL, Yu SP, Wei L. Cell death and proliferation in NF-kappaB p50 knockout mouse after cerebral ischemia. Brain Res. 2008; 1230:281–289. [PubMed: 18657523]

Liu HT, Tashmukhamedov BA, Inoue H, Okada Y, Sabirov RZ. Roles of two types of anion channels in glutamate release from mouse astrocytes under ischemic or osmotic stress. Glia. 2006; 54:343–357. [PubMed: 16883573]

Lu ZY, Yu SP, Wei JF, Wei L. Age-related neural degeneration in nuclear-factor kappaB p50 knockout mice. Neuroscience. 2006; 139:965–978. [PubMed: 16533569]

Maly FE, Schuerer-Maly CC, Quilliam L, Cochrane CG, Newburger PE, Curnutte JT, Gifford M, Dinauer MC. Restitution of superoxide generation in autosomal cytochrome-negative chronic granulomatous disease (A22(0) CGD)-derived B lymphocyte cell lines by transfection with p22phax cDNA. J Exp Med. 1993; 178:2047–2053. [PubMed: 8245781]

McCarthy KD, de Vellis J. Preparation of separate astroglial and oligodendroglial cell cultures from rat cerebral tissue. J Cell Biol. 1980; 85:890–902. [PubMed: 6248568]

Moore SF, MacKenzie AB. NADPH oxidase NOX2 mediates rapid cellular oxidation following ATP stimulation of endotoxin-primed macrophages. J Immunol. 2009; 183:3302–3308. [PubMed: 19696433]

Papa S, Zazzeroni F, Pham CG, Bubici C, Franzoso G. Linking JNK signaling to NF-kappaB: a key to survival. J Cell Sci. 2004; 117:5197–5208. [PubMed: 15483317]

Park L, Anrather J, Girouard H, Zhou P, Iadecola C. Nox2-derived reactive oxygen species mediate neurovascular dysregulation in the aging mouse brain. J Cereb Blood Flow Metab. 2007; 27:1908–1918. [PubMed: 17429347]

Pfrieger FW, Barres BA. Synaptic efficacy enhanced by glial cells in vitro. Science. 1997; 277:1684–1687. [PubMed: 9287225]

Quinones MP, Kalkonde Y, Estrada CA, Jimenez F, Ramirez R, Mahimainathan L, Mummidi S, Choudhury GG, Martinez H, Adams L, Mack M, Reddick RL, Maffi S, Haralambous S, Probert L, Ahuja SK, Ahuja SS. Role of astrocytes and chemokine systems in acute TNFalpha induced demyelinating syndrome: CCR2-dependent signals promote astrocyte activation and survival via NF-kappaB and Akt. Mol Cell Neurosci. 2008; 37:96–109. [PubMed: 17949991]

Raad H, Paclet MH, Boussetta T, Kroviarski Y, Morel F, Quinn MT, Gougerot-Pocidalo MA, Dang PM, El-Benna J. Regulation of the phagocyte NADPH oxidase activity: phosphorylation of gp91phox/NOX2 by protein kinase C enhances its diaphorase activity and binding to Rac2, p67phox, and p47phox. FASEB J. 2009; 23:1011–1022. [PubMed: 19028840]

Raz L, Zhang QG, Zhou CF, Han D, Gulati P, Yang LC, Yang F, Wang RM, Brann DW. Role of Rac1 GTPase in NADPH oxidase activation and cognitive impairment following cerebral ischemia in the rat. PLoS One. 5:e12606. [PubMed: 20830300]

Reigada D, Lu W, Zhang M, Mitchell CH. Elevated pressure triggers a physiological release of ATP from the retina: Possible role for pannexin hemichannels. Neuroscience. 2008; 157:396–404. [PubMed: 18822352]

Reinehr R, Gorg B, Becker S, Qvartskhava N, Bidmon HJ, Selbach O, Haas HL, Schliess F, Haussinger D. Hypoosmotic swelling and ammonia increase oxidative stress by NADPH oxidase in cultured astrocytes and vital brain slices. Glia. 2007; 55:758–771. [PubMed: 17352382]

Saijo K, Winner B, Carson CT, Collier JG, Boyer L, Rosenfeld MG, Gage FH, Glass CK. A Nurr1/CoREST pathway in microglia and astrocytes protects dopaminergic neurons from inflammation-induced death. Cell. 2009; 137:47–59. [PubMed: 19345186]

Schneider A, Martin-Villalba A, Weih F, Vogel J, Wirth T, Schwaninger M. NF-kappaB is activated and promotes cell death in focal cerebral ischemia. Nat Med. 1999; 5:554–559. [PubMed: 10229233]

Schousboe A, Divac I. Difference in glutamate uptake in astrocytes cultured from different brain regions. Brain Res. 177:407–409. [PubMed: 497842]

Schummers J, Yu H, Sur M. Tuned responses of astrocytes and their influence on hemodynamic signals in the visual cortex. Science. 2008; 320:1638–1643. [PubMed: 18566287]

Taille C, El-Benna J, Lanone S, Dang MC, Ogier-Denis E, Aubier M, Boczkowski J. Induction of heme oxygenase-1 inhibits NAD(P)H oxidase activity by down-regulating cytochrome b558 expression via the reduction of heme availability. J Biol Chem. 2004; 279:28681–28688. [PubMed: 15123630]

Takahashi Y, Katai N, Murata T, Taniguchi SI, Hayashi T. Development of spontaneous optic neuropathy in NF-kappaBetap50-deficient mice: requirement for NF-kappaBetap50 in ganglion cell survival. Neuropathol Appl Neurobiol. 2007; 33:692–705. [PubMed: 17931357]

Tezel G, Wax MB. Increased production of tumor necrosis factor-alpha by glial cells exposed to simulated ischemia or elevated hydrostatic pressure induces apoptosis in cocultured retinal ganglion cells. J Neurosci. 2000; 20:8693–8700. [PubMed: 11102475]

Toft-Hansen H, Fuchtbauer L, Owens T. Inhibition of reactive astrocytosis in established experimental autoimmune encephalomyelitis favors infiltration by myeloid cells over T cells and enhances severity of disease. Glia. 59:166–176. [PubMed: 21046558]

Uno H, Matsuyama T, Akita H, Nishimura H, Sugita M. Induction of tumor necrosis factor-alpha in the mouse hippocampus following transient forebrain ischemia. J Cereb Blood Flow Metab. 1997; 17:491–499. [PubMed: 9183286]

Yoshioka H, Niizuma K, Katsu M, Okami N, Sakata H, Kim GS, Narasimhan P, Chan PH. NADPH oxidase mediates striatal neuronal injury after transient global cerebral ischemia. J Cereb Blood Flow Metab.

Yu L, Zhen L, Dinauer MC. Biosynthesis of the phagocyte NADPH oxidase cytochrome b558. Role of heme incorporation and heterodimer formation in maturation and stability of gp91phox and p22phox subunits. J Biol Chem. 1997; 272:27288–27294. [PubMed: 9341176]

Zhao Y, Rempe DA. Targeting astrocytes for stroke therapy. Neurotherapeutics. 2010; 7:439–451. [PubMed: 20880507]

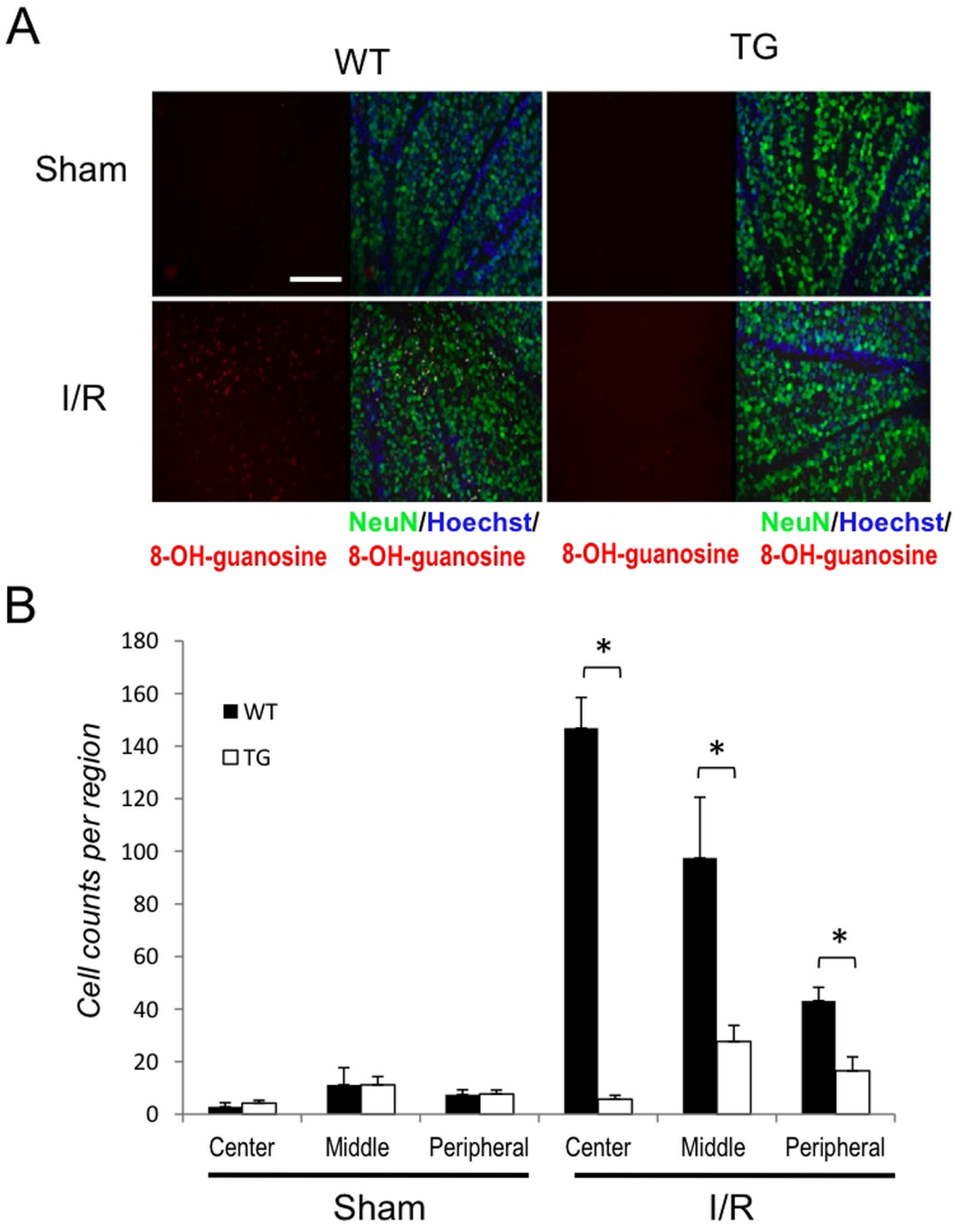

Figure 1. Inhibition of astroglial NF-κB reduces oxidative stress following retinal IR injury

(**A**) Representative images showing DNA/RNA damage localizing to NeuN-positive cells detected by 8-OH-guanosine (red) immunofluoresent labeling. Double-labeled cells are abundant in the GCL of the central retina 3 days after IR injury. Scale bar, 100 mm (**B**) Quantification of DNA/RNA damage; total counts of 8-OH-guanosine/NeuN/Hoechst-positive cells were averaged from the sum of 4 standard fields in each retinal region. Values are means ± SEM, n=6; *p<0.05.

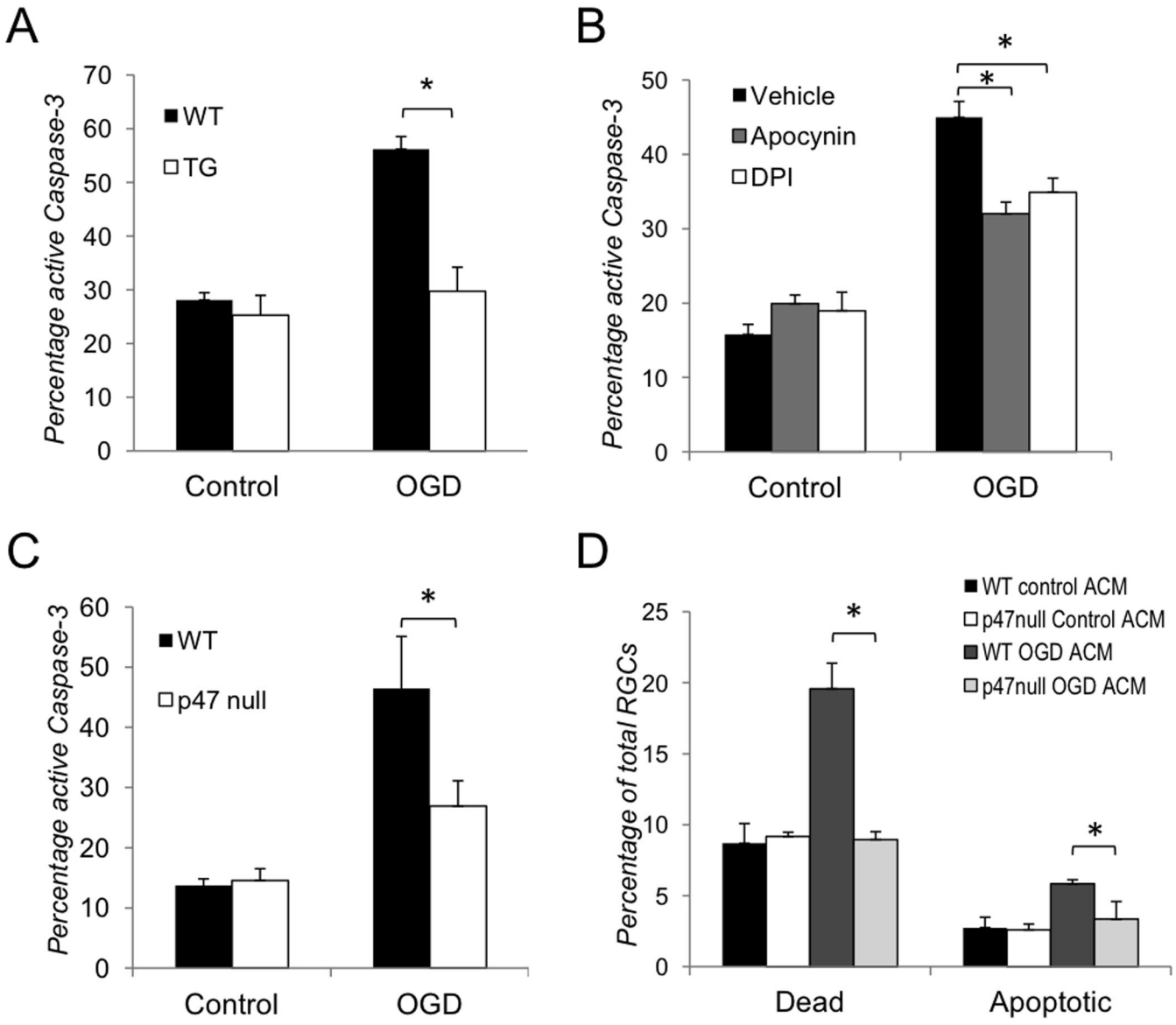

Figure 2. Inhibition of aNF-κB promotes survival of retinal ganglion cells *in vitro* after OGD

(**A–C**) Quantification of active caspase-3 positive RGCs in co-culture with astrocytes 24 hours after OGD challenge (OGD) vs. normoxic controls (Control) performed by confocal microscopy. The total quantities of NeuN or beta-III tubulin/Hoechst positive RGCs observed in 5 randomly selected fields of each experimental plate are compared. Values are means ± SEM, n=5; *p<0.05. **(A)** Activated caspase-3 positive RGCs in co-culture with WT and TG astrocytes; **(B)** Activated caspase-3 positive WT RGC in co-cultures with astrocytes treated with the NADPH oxidase inhibitors DPI (1μM) or apocynin (100μM); **(C)** Activated caspase-3 positive RGCs in co-cultures of WT astrocytes with WT or $p47^{null}$ RGCs **(D)** Cell death rates in WT and $p47^{null}$ RGCs challenged by astrocyte-conditioned media (ACM) from primary astrocytes subjected to OGD challenge (OGD ACM) or from normoxic control astrocytes (Control ACM). The percentages of dead (PI/Hoechst positive) and apoptotic (Annexin V/Hoechst positive) RGCs in ACM-treated cultures were calculated relative to total quantities of Hoechst positive cell in 5 randomly selected fields. Values are means ± SEM, n=5; *p<0.05.

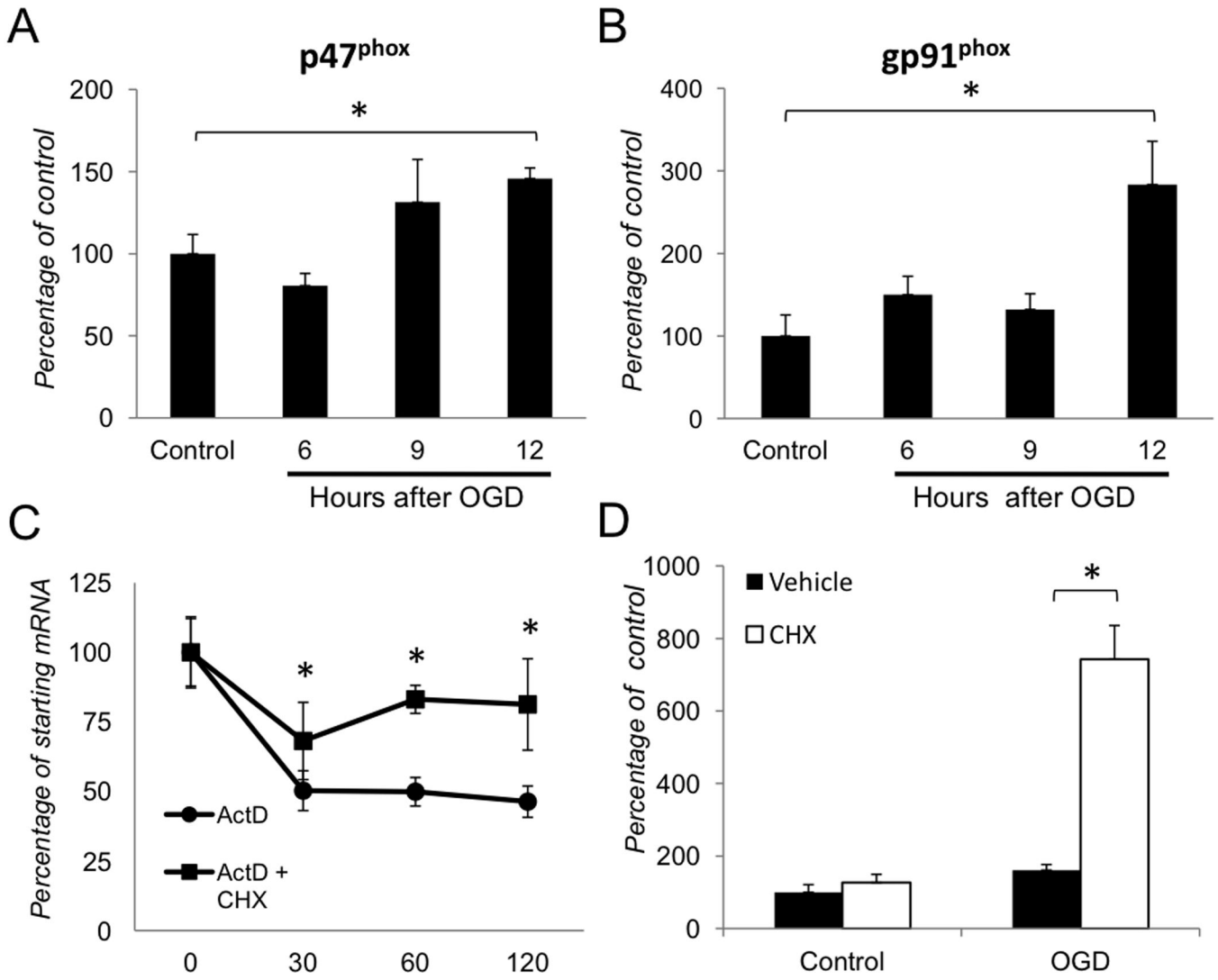

Figure 3. Transcriptional regulation of NADPH oxidase following OGD in primary astrocytes

(**A–B**) Gene expression analysis of the $p47^{PHOX}$ and $gp91^{PHOX}$ genes 6, 9 and 12 hours after OGD challenge. Changes were calculated as percentages of untreated control (Control) value. (**C**) Analysis of $p47^{PHOX}$mRNA decay in actinomysin D (5μg/ml) treated cells with or without cycloheximide (5μg/ml) 12 hours after OGD treatment. (**D**) Relative abundance of $p47^{PHOX}$ transcript levels in astrocytes treated with vehicle or cycloheximide (5μg/ml). Gene expression levels were normalized to β-actin. Values are means ± SEM, n=4 and *p<0.05.

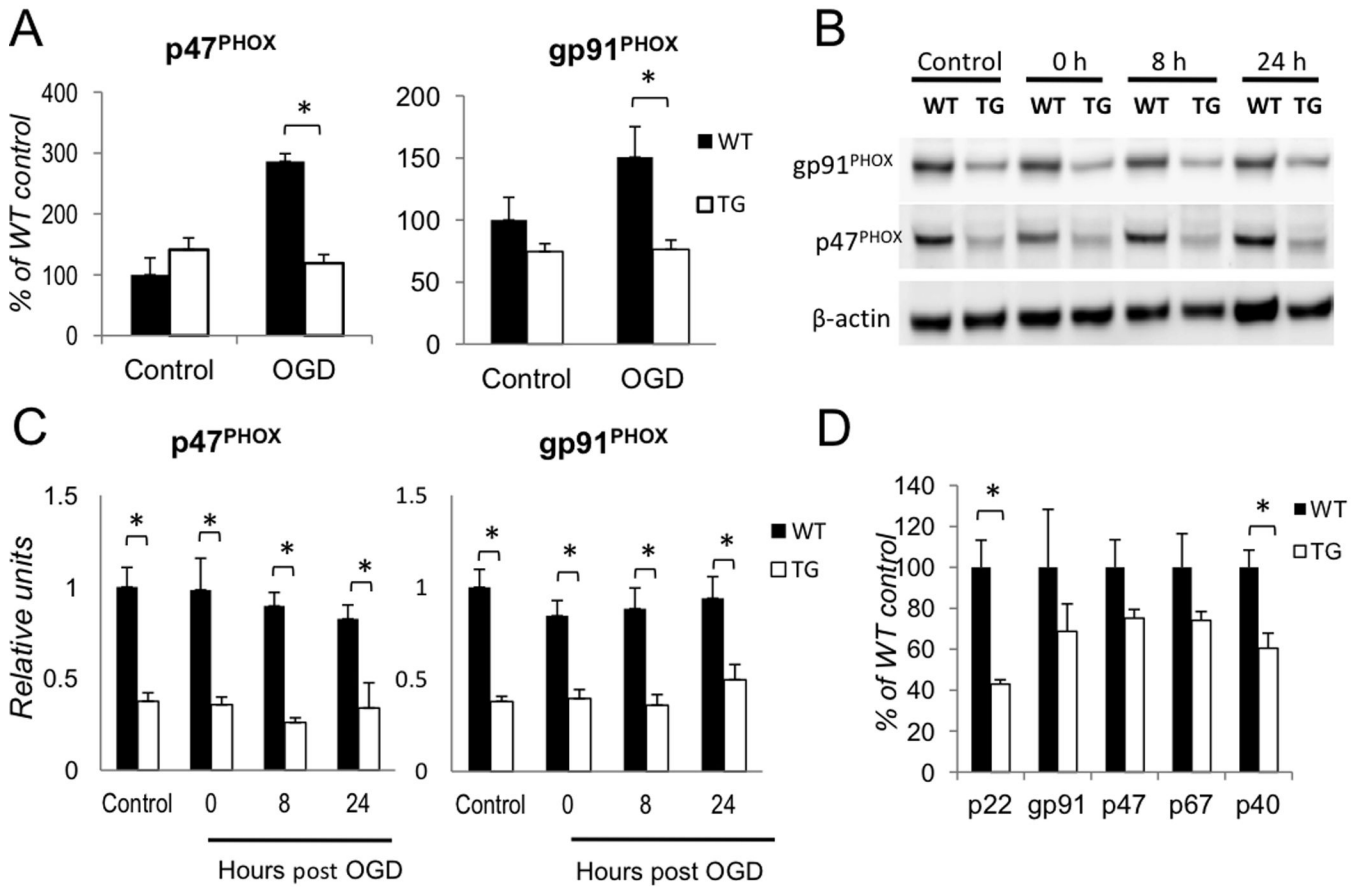

Figure 4. Regulation of homeostatic levels of PHOX is NF-κB dependent

(A) Gene expression analysis of gp91^{PHOX} and p47^{PHOX} transcripts 12 hours after OGD. Changes were calculated as percentages of untreated WT control (Control) values (n=5, *p<0.05). **(B)** Time course analysis of gp91^{PHOX}and p47^{PHOX}protein levels after OGD by quantitative western blot. **(C)** Quantification of the data shown in (B): the gp91^{PHOX} and p47^{PHOX} band intensities were normalized to β-actin (n=3, *p<0.05). **(D)** Relative expression levels of genes encoding PHOX subunit in untreated WT and TG astrocytes (n=5; p<0.01).

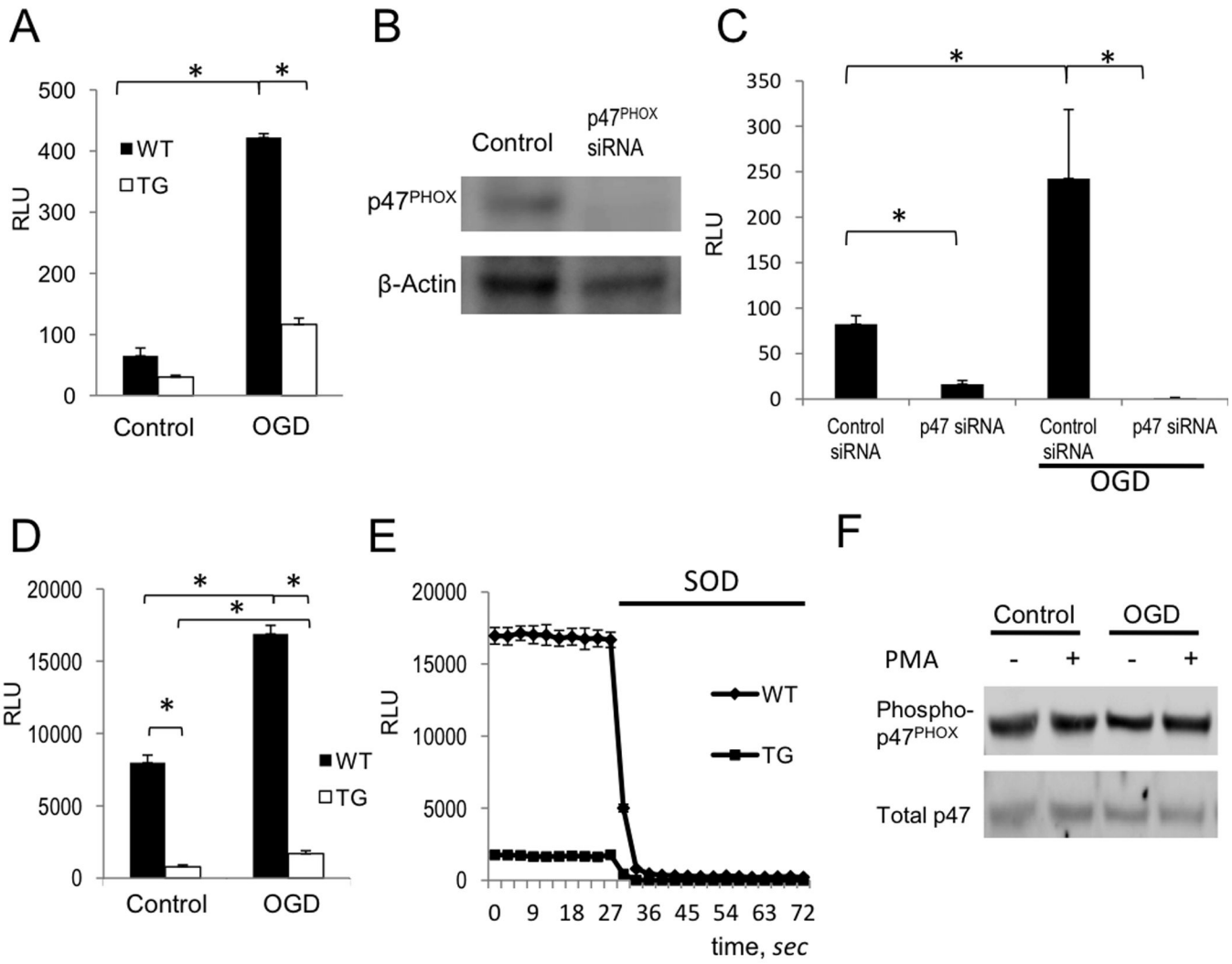

Figure 5. ROS production by PHOX in astrocytes is regulated by NF-κB

(A) WT and TG astrocytes were assayed for superoxide production by Diogenes luminescence in control cultures and 24 hours after OGD challenge (OGD) (RLU = relative light units; n=5, $p<0.05$). **(B)** Transfection of $p47^{PHOX}$ siRNA reduces $p47^{PHOX}$ protein levels. Cell lysates were analyzed by western blot 24 hours post-transfection. **(C)** ROS production in live astrocytes was detected by Diogenes chemiluminescence 24 hours following OGD in non-targeting control siRNA (control) and $p47^{PHOX}$siRNA transfected cells. Astrocytes were transfected with siRNA 24 hours prior to OGD treatment. (n=5, *$p<0.01$). **(D)** Analysis of ROS production in WT and TG astrocytes 20 minutes after addition of PMA (1ng/ml) in control cultures and 24 hours after OGD (n=5, *$p<0.01$). **(E)** Representative recordings of ROS production from **(D)** in WT vs TG cells. Chemiluminesence was quenched by the addition of SOD (20U/ml). **(F)** Analysis of $p47^{PHOX}$ phosphorylation status by western blot in primary astrocyte extracts. OGD challenged and control astrocytes were treated with DMSO vehicle or PMA (1ng/ml) for 20 minutes prior to cell lysis.

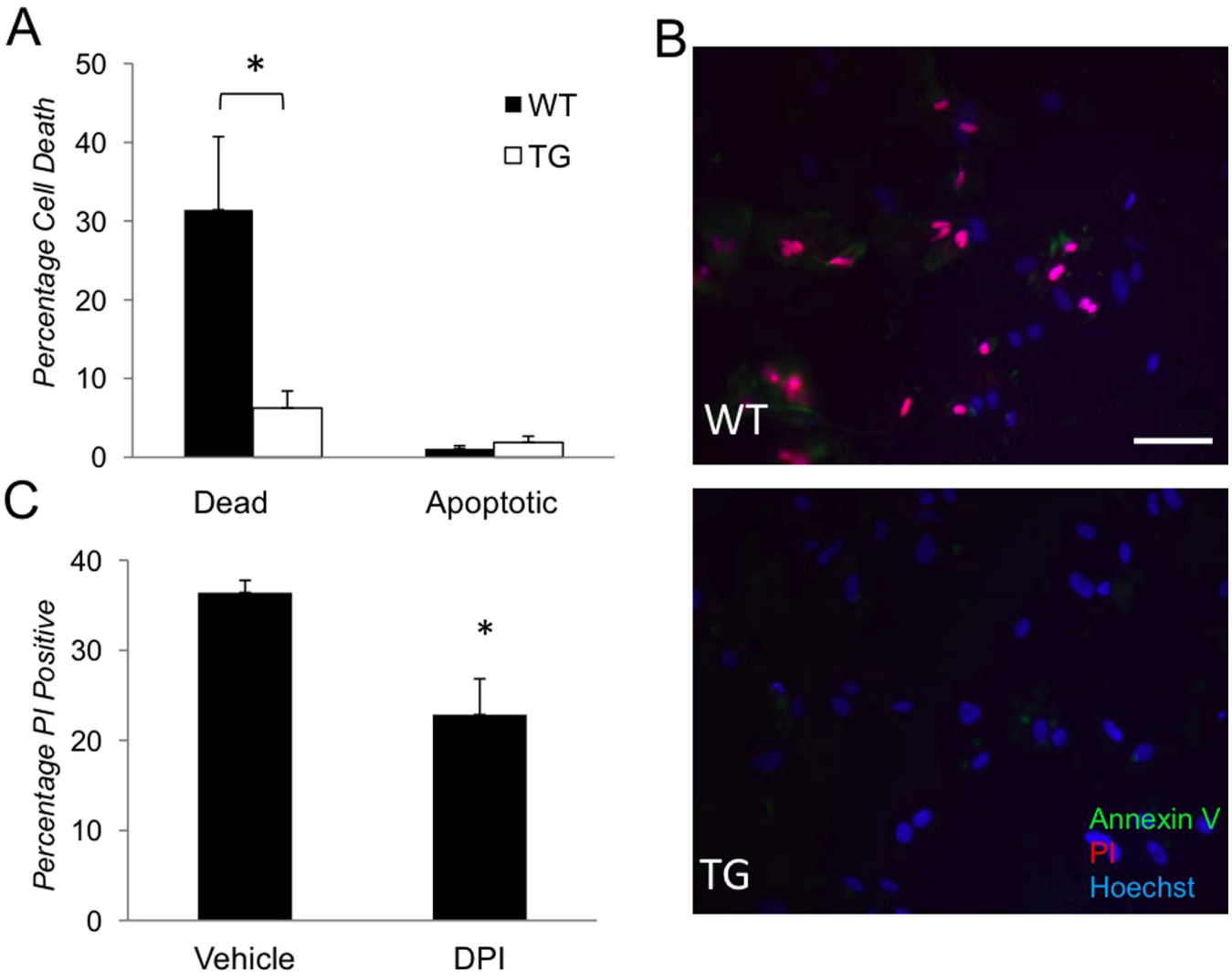

Figure 6. The effects of NF-κB and PHOX suppression on OGD-induced cell death in primary astrocytes

(A–B) Cell death rates in cultures determined by quantification of cells with PI (red) and AnnexinV (green) labeling 24 hours after OGD (n=3, *p<0.05). **(B)** Representative images from experiment **A** showing abundant dead (PI-positive or PI/AnnexinV-positive) cells in WT but not in TG cultures; Hoechst dye (blue) labels nuclei for total cell counts. **(C)** Cell death rates (% of PI- positive among Hoechst- positive) cells in vehicle-treated control and 1μM DPI-treated astrocytes cultures 24 hours after OGD (n=4, *p<0.05). Scale bar 50μm.